Structural Variation of Silver Clusters from Ag_{13} to Ag_{160}

Xiaoli Yang, Wensheng Cai, and Xueguang Shao*

State Key Laboratory of Functional Polymer Materials for Adsorption and Separation, Research Center for Analytical Sciences, Department of Chemistry, Nankai University, Tianjin, 300071, People's Republic of China

Received: February 12, 2007; In Final Form: April 8, 2007

The structures of silver clusters from Ag_{121} to Ag_{160} were optimized with a modified dynamic lattice searching (DLS) method, named as DLS with constructed core (DLSc). The interaction among silver atoms is modeled by the Gupta potential. Structural characteristic of silver clusters with the growth of cluster size is investigated with the newly optimized structures and our previous results from Ag_{13} to Ag_{120}. A set of amorphous structures was obtained in the size range of 13−48, together with several ordered structures. The putative stable motif is an icosahedron from Ag_{49} to Ag_{61} and then changes to a decahedron in the size range of 62−160. Some of the results are consistent with experiments. Furthermore, it was also found that, for clusters with decahedral motif, the stable structure is a result of the competition among the different Marks decahedral motifs. On the other hand, different from the Lennard-Jones cluster, there are some silver clusters with the face-centered cubic (fcc) motif in the size range of 13−160. But the fcc motif can only be obtained for some specific sizes.

1. Introduction

There have been great interests in experimental and theoretical investigations of small silver cluster due to its applications in photography, catalysis, electronic materials, surface nanostructuring, etc.[1−6] The study of the structural changes of small (tens through hundreds of atoms) silver clusters with their sizes is a hotpot because it may reveal the relationship between structures and their physical and chemical properties.[7,8]

In experiments, the observed structure of a silver cluster is a result of the competition between thermodynamic and kinetic factors.[9−12] At small size, silver clusters take the forms of icosahedral (Ih), truncated Marks decahedral (*m*-Dh), face-centered cubic (fcc), and amorphous motifs. Many experiments and theoretical studies have been devoted to determination of the putative stable structures depending on the cluster size. In 1991, Hall et al.[9] studied the structures of small silver clusters grown in inert gas aggregation (IGA)[13] source using electron diffraction. Ih, Dh, and fcc clusters between 2 and 4 nm diameter were observed. It was found that the relative proportions of these motifs depend on experimental conditions, and for small clusters (∼2 nm of diameter, corresponding to 100−200 atoms), the structures are mainly in Dh motif. Then, in 1997, Reinhard et al.[10] studied the size-independent fcc-to-icosahedron structural transition of large silver clusters grown in IGA source up to 11 nm in diameter. On the basis of these works, Baletto et al.[11,14,15] did a series of works on theoretical simulation of the silver clusters. In 2000, they studied the growth of free silver clusters up to 150 atoms by molecular dynamics simulation from a small seed.[11] It was shown that Dh is the most possible motif in the most experimental conditions, but Ih structures are indeed energetically favorable. In 2001, they investigated the growth of silver clusters up to 600 atoms by molecular dynamics simulation on realistic time scales and in a temperature range from 400 to 650 K.[14] At low and intermediate temperatures (350 $< T <$ 500 K), the clusters grow through a sequence from Ih to Dh and then back to Ih. The first Ih to Dh transition takes place always in the size range of 55−75, while the crucial transformation from Dh to Ih takes place around Ag_{100} if $T <$ 400 K and around Ag_{200} if $T >$ 400 K. At high temperatures ($T >$ 600 K), most of the clusters take the structural motif of fcc, after passing through a Dh regime around Ag_{200}. Then, they studied the crossover size among structural motifs, which showed that the best motif is Ih for the clusters size smaller than 147, Dh in the size range of 300−20 000, and fcc at much larger size.[15] Finally, they explained the silver cluster structures by energy, thermodynamics and kinetics.[12] These simulations provided a great help for a deep understanding of the experimental observations. Moreover, other works on theoretical analysis of silver clusters have also been reported.[16−21]

On the other hand, optimization algorithms, such as the evolutionary algorithm,[22] random tunneling algorithm (RTA),[23] and dynamic lattice searching (DLS) methods[24] have been developed to study the putative stable structures and the corresponding lowest potential energies of silver clusters at given sizes. However, limited by the efficiency of the algorithms, only small silver clusters or the clusters with given specific sizes were optimized, e.g., in the work of Baletto et al.,[15] only the energies of the silver clusters at the magic numbers were investigated. The optimization of silver clusters in a consecutive size range is still scarce. In our previous works,[23,24] the putative stable structures of silver clusters up to 80 atoms and from 61 to 120 atoms were studied, respectively. It was found that the dominating motifs are disordered morphologies in the size range of 15−47, Ih in the size range of 48−54, and the dominating motif changes from Ih to Dh in the size range of 55−75. It was also found that, from Ag_{61} to Ag_{120}, the majority of the clusters have Dh motif, and these results are found to be consistent with experimental results of Hall,[9] but different to the theoretical results of Baletto.[15]

In this work, a modified DLS[25,26] method, named as DLS with constructed core (DLSc),[27] was used to optimize the structures of the silver clusters from Ag_{121} to Ag_{160}. It was found that the majority of the structures in this size range are also

* To whom correspondence should be addressed. Phone: +86-22-23503430. Fax: +86-22-23502458. E-mail: xshao@nankai.edu.cn.

10.1021/jp0711895 CCC: $37.00
Published on Web 05/22/2007

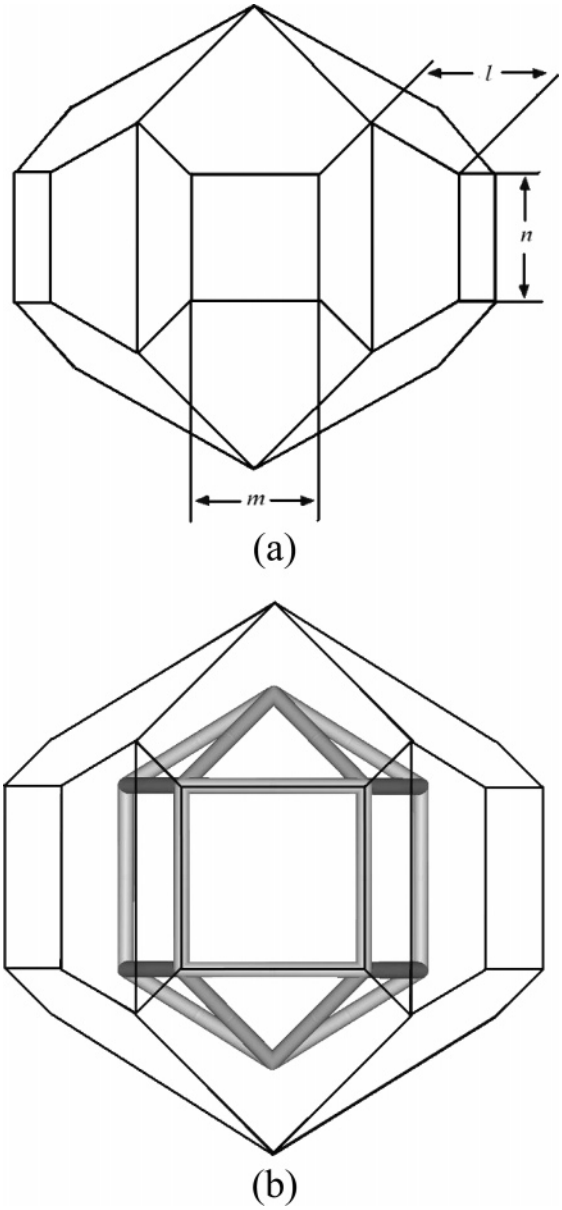

Figure 1. Configuration of (a) Ino decahedron and (b) *m*-Dh. *m* and *n* are width and height of the rectangular (100) facets, respectively, while *l* is the depth of the Marks re-entrance.

Dh, but there are Ih and fcc structures, which is consistent with the explanation of Baletto et al.[12] Together with the previous results of Ag_{13-120}, structural characteristic of Ag_{13-160} are investigated in detail for a better understanding of the changing rule of the structures with the cluster size. Results show that, with the growth of the cluster size, the dominant structural motif changes from amorphous ($Ag_{13}-Ag_{48}$) to Ih ($Ag_{49}-Ag_{61}$) and then to Dh ($Ag_{62}-Ag_{160}$). Furthermore, the clusters with Dh motif were classified into different kinds of *m*-Dh submotifs. The Dh structure of a given cluster was found to be a result of the competition among different *m*-Dh submotifs.

2. Method

The DLS method was proposed by combining the basic ideas of unbiased and biased methods.[25,26] A DLS run starts from a randomly generated and locally minimized structure of a cluster, and then repetitively finds structures with lower energy by "lattice construction" and "lattice searching". The former operation constructs all possible vacant sites around the starting structure, and the latter operation finds structures with lower energy by moving the atoms with higher energy to the vacant sites with lower energy. The merit of the DLS method is that, by using dynamic lattice strategy, the searching space is greatly reduced. However, with the increase of the cluster size, the searching space will increase too. For optimization of large clusters, further reduction of the searching space is still needed. With a simple consideration that the searching space can be reduced by reducing the number of atoms involved in the optimization, DLSc was proposed.[27] In the DLSc method, instead of generating the starting structure randomly, an inner core is used to generate the starting structure. Only the atoms in outer layers are involved in lattice searching. Thus, the searching space is further reduced compared with that in the previous DLS.

For silver clusters, there are mainly three kinds of ordered structural motifs, i.e., Ih, Dh, and fcc. So, in this study, Ih, Dh, and fcc inner cores are used, respectively, in the DLSc method. The Ih core was obtained by constructing the Ih lattices with the method in ref 27. For *m*-Dh motif, its structure can be described with three parameters, *m*, *n*, *l*, where, as shown in Figure 1a, *m* and *n* are the width and the height of the rectangular (100) facets, respectively, and *l* is the depth of the Marks reentrance.[28,29] Therefore, an *m*-Dh structure can be described by (*m*, *n*, *l*). At the same time, an Ino Dh can be taken as an inner core of an *m*-Dh, because it can be obtained by moving out the atoms in the outer shells from an *m*-Dh (as shown in Figure 1b). Therefore, in this work, Ino Dh structure was used as a kind of core in DLSc for *m*-Dh motifs, and it was constructed by the method in ref 30. Furthermore, because fcc structures, including the truncated octahedron (TO), were found in silver clusters, fcc octahedron was also used as a kind of core, and it was constructed by the method in ref 30. Therefore, Ino Dh, Ih, and fcc octahedron were used as the inner cores of the starting structure in DLSc. The final result was obtained by choosing the structure with the lowest energy among the independent runs with different cores.

On the other hand, different semiempirical potentials have been proposed for transition and noble metallic clusters, such as effective-medium theory,[31] the glue model,[32] embedded-atom,[33] Sutton−Chen,[34] Rosato−Guillope−Legrand (RGL),[35] and the Gupta potential.[36] The later one was used in this work. Gupta potential is based on the second moment approximation of the electron density of states in the tight-binding (TB) theory. It can be depicted in the following form[36]

$$V = \frac{U_N}{2} \sum_{i=1}^{N} V_i \tag{1}$$

where N is the number of atoms in the cluster and U_N is a function of the atom number N. V_i consists of a pairwise repulsion energy of Born−Mayer type and a N-body attractive contribution

$$V_i = A \sum_{j \neq i} \exp\left[-p\left(\frac{r_{ij}}{r_0} - 1\right)\right] - \left(\sum_{j \neq i} \exp\left[-2q\left(\frac{r_{ij}}{r_0} - 1\right)\right]\right)^{1/2} \tag{2}$$

r_{ij} is the distance between atom i and j, and r_0 is the equilibrium nearest-neighbor distance in the bulk metal. The parameters p and q represent the repulsive and the attractive interaction range, respectively. The parameter A is fitted to experimental values

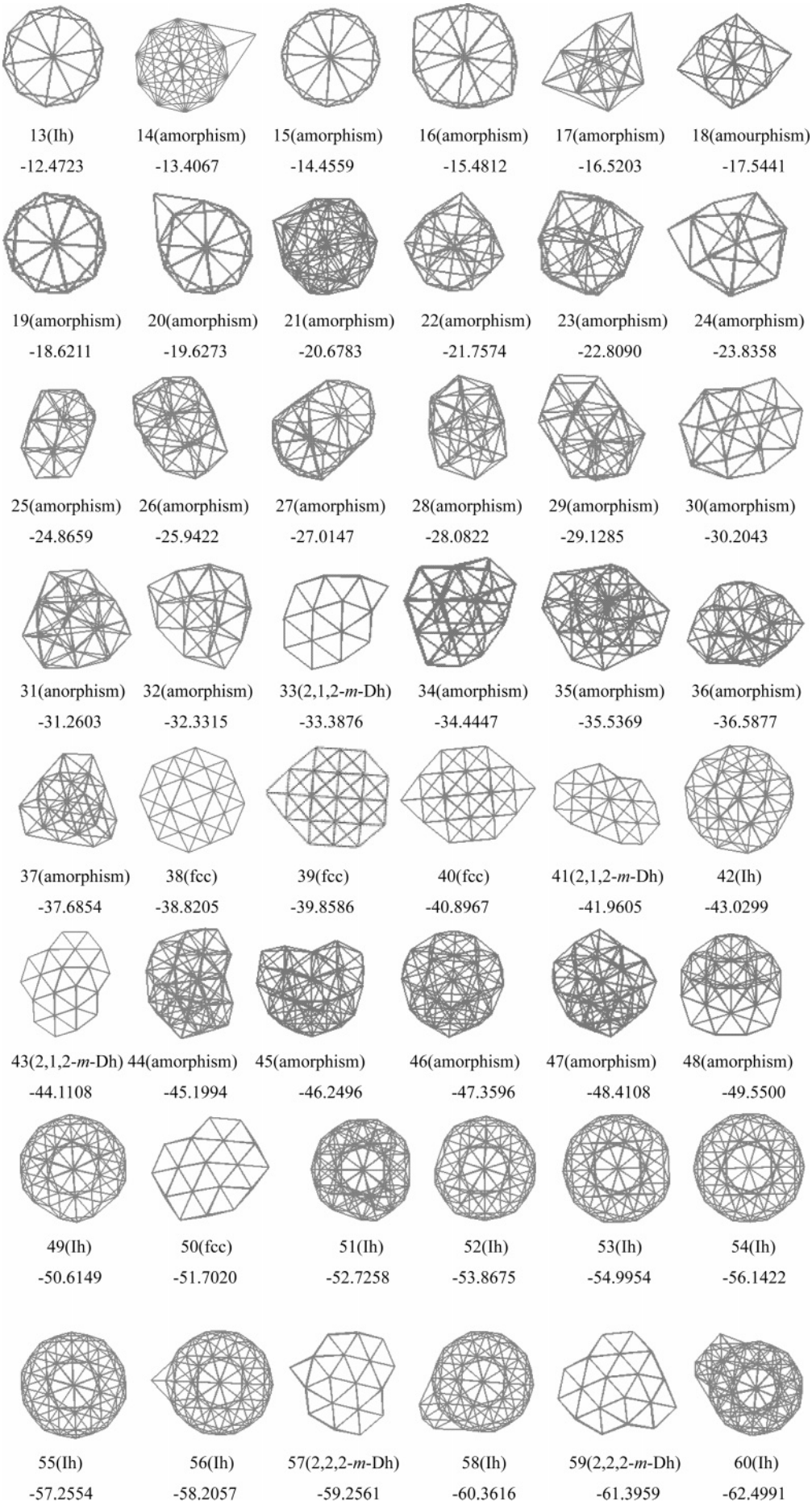

Figure 2. Part 1 of 4.

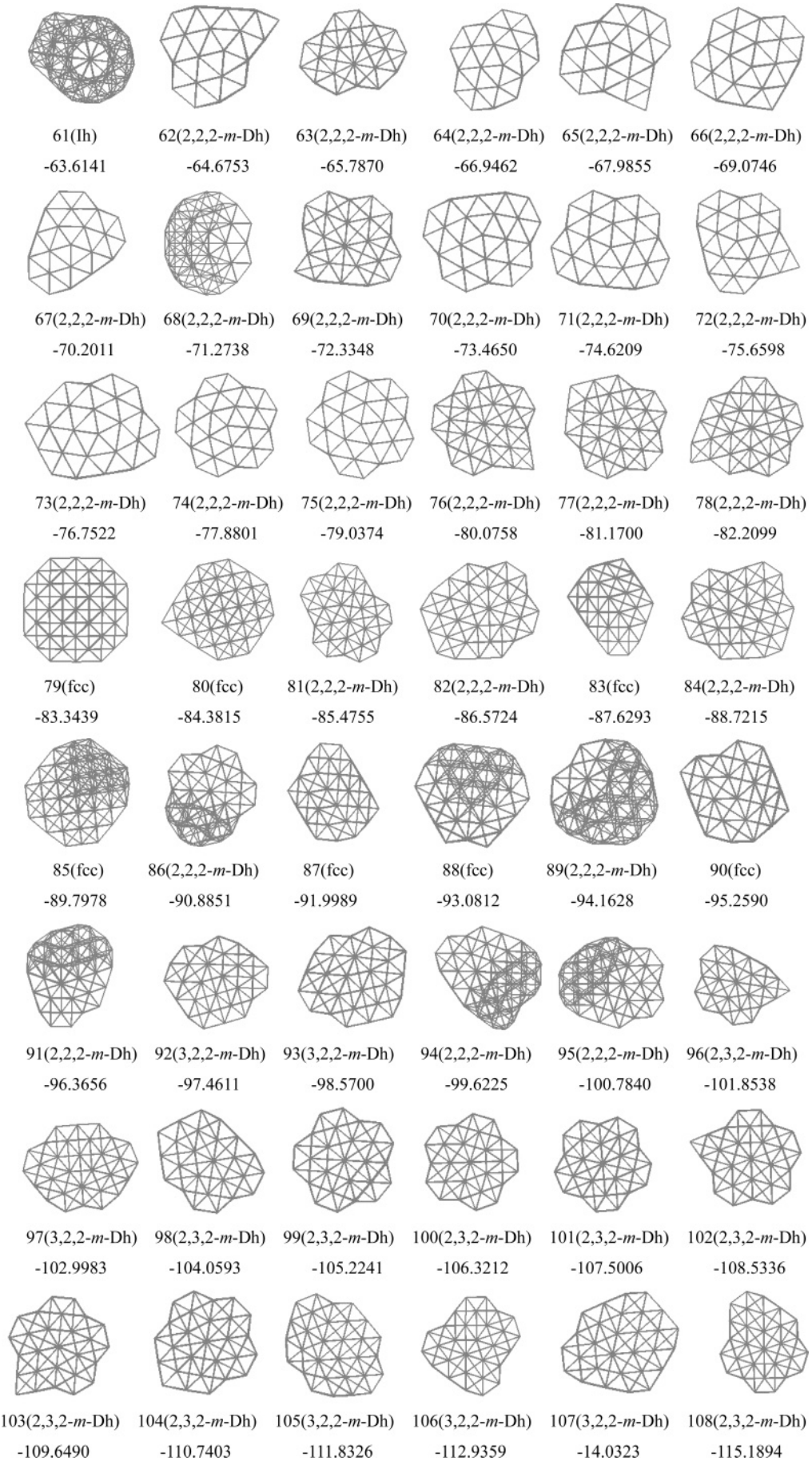

Figure 2. Part 2 of 4.

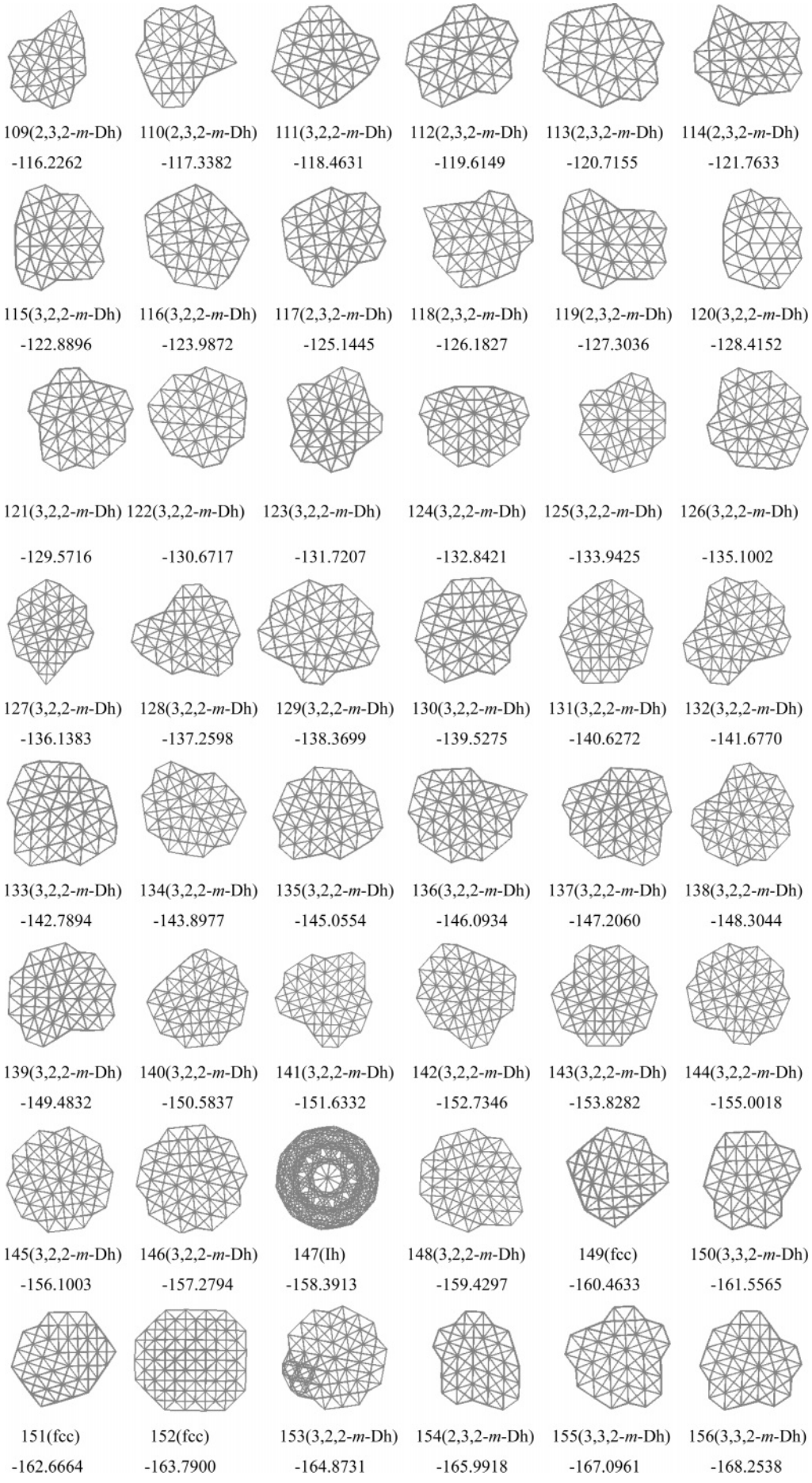

Figure 2. Part 3 of 4.

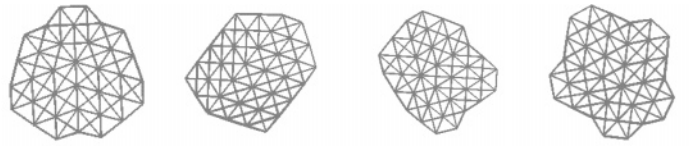

Figure 2. Part 4 of 4. Optimized structures, structural motifs, and the corresponding potential energies of the silver clusters from Ag_{13} to Ag_{160}.

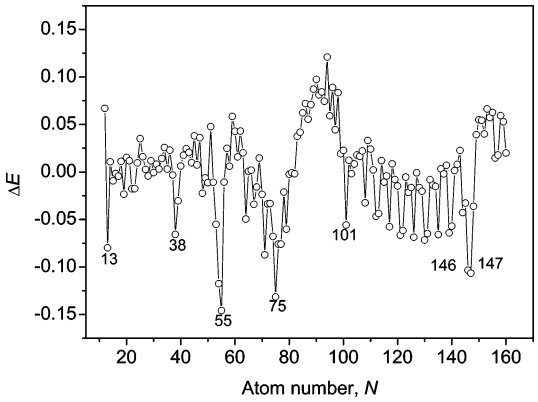

Figure 3. The finite difference (ΔE) of the energy of silver clusters from Ag_{13} to Ag_{160} for $E_{J(N)} = -0.92253 + 0.81546N^{1/3} + 0.29672N^{2/3} - 1.15599N$.

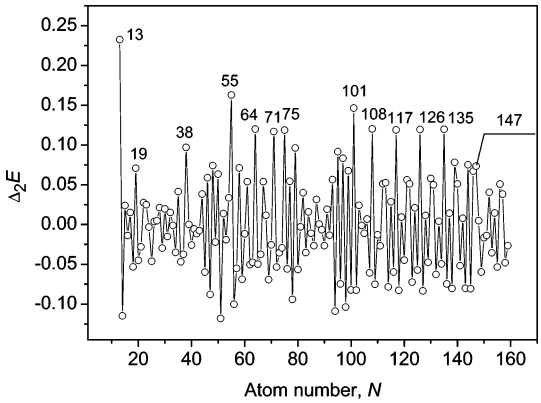

Figure 4. The second finite difference ($\Delta_2 E$) of the energy of silver clusters from Ag_{13} to Ag_{160}.

of the cohesive energy. In this work, $A = 0.09944$, $p = 10.12$, $q = 3.37$, and the reduced units with $r_0 = 1$ and $U_N = 1$ were used.[34]

3. Results and Discussion

3.1. Putative Stable Structures of the Silver Clusters up to 160 Atoms. Figure 2 shows the optimized structures and the corresponding lowest energies of silver clusters from Ag_{13} to Ag_{160}. Among these structures, $Ag_{13}-Ag_{120}$ were obtained with RTA and DLS methods, respectively, in our previous work,[23,24] and $Ag_{121}-Ag_{160}$ were obtained with DLSc method in this work. It can be seen that, in the size range of 121−160, Dh is the dominant motif; only one Ih structure is obtained at Ag_{147} and four fcc structures are obtained at the size of $N = 149$, 151, 152, and 158. This result is consistent with the results of the experiment and theoretical simulation.[9,11] In the experiment of ref 9, the silver clusters are found to be mainly *m*-Dh in the range of 100−200, and, in the theoretical study of ref 11, it was found that the silver clusters up to 150 atoms are most possibly *m*-Dh.

3.2. Variation of the Structures and Energies with Size. Figures 3 and 4 shows the finite difference of energy ΔE and the second finite difference of energy $\Delta_2 E$ as a function of cluster size N, respectively. The ΔE and $\Delta_2 E$ have the form as follows

$$\Delta E_{(N)} = E_{(N)} - E_{J(N)} \tag{3}$$

$$\Delta_2 E_{(N)} = E_{(N+1)} + E_{(N-1)} - 2E_{(N)} \tag{4}$$

where $E_{J(N)} = a + bN^{1/3} + cN^{2/3} + dN$ is a four-parameter fit of the energy of global minimum. Clearly, ΔE shows the variation of the cluster stability with cluster size, and $\Delta_2 E$ measures the stability of an N-atom cluster structure with respect to its neighboring cluster size. The negative peaks (or valleys) in Figure 3 and the positive peaks in Figure 4 indicate particularly stable structures comparing to their neighbors.

At first, in Figure 3, seven apparent valleys at Ag_{13}, Ag_{38}, Ag_{55}, Ag_{75}, Ag_{101}, Ag_{146}, and Ag_{147} can be clearly found, which correspond to the complete structural motifs or the magic number clusters. Figure 5 shows the top view and side view of these structures. In more detail, from Ag_{14} to Ag_{48}, the value of ΔE goes up very slightly with fluctuation except for the valley at Ag_{38}. The dominant motif in this size range is disordered structure, but the structural motif is fcc for Ag_{38}, Ag_{39}, and Ag_{40}. Another negative peak in Figure 3 can be found around Ag_{55} from Ag_{49} to Ag_{61}. In this range, the dominant motif is Ih, and

TABLE 1: Structural Distribution of $Ag_{13}-160$ Clusters

structural motif		n[a]	*cluster size (N)*
amo rphi sm		28	14−32, 34−37, 44−48
Ih		13	13, 42, 49, 51−56, 58, 60, 61, 147
fcc		15	38−40, 50, 79, 80, 83, 85, 87, 88, 90, 149, 151, 152, 158
Dh	*(2,1,2) m*-Dh	3	33, 41, 43
	(2,2,2) m-Dh	27	57, 59, 62−78, 81, 82, 84, 86, 89, 91, 94, 95
	(2,3,2) m-Dh	18	96, 98−104, 108−110, 112−114, 117−119, 154
	(3,2,2) m-Dh	39	92, 93, 97, 105−107, 111, 115, 116, 120-146, 148, 153, 160
	(3,3,2) m-Dh	5	150, 155−157, 159

[a] Total number of the motif.

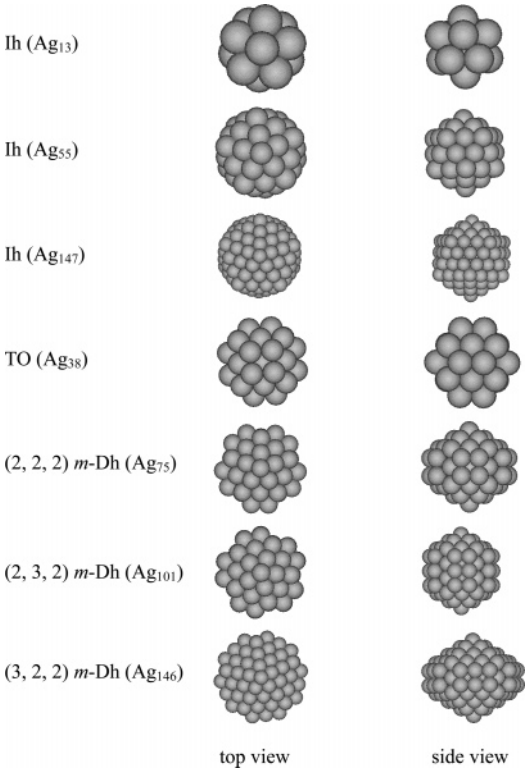

Figure 5. The top and side views of the silver cluster structures at magic numbers.

Ag_{55} is a complete Ih structure. However, the structural motif is fcc for Ag_{50} and (2,2,2) *m*-Dh for Ag_{57} and Ag_{59}. The clusters from Ag_{51} to Ag_{54} are more and more stable because that the structures gradually approach to the complete Ih structure, but the symmetry of Ag_{56} is destroyed by one extra atom in the out shell compared with the Ag_{55} complete Ih structure. Therefore, the negative peak is a reflection of the growth of Ih structure. When $N \geq 62$, the ΔE goes down with fluctuation and then goes up after $N = 75$ until $N = 95$. In this size range, the domain motif is (2, 2, 2) *m*-Dh and Ag_{75} is a complete one. After $N = 96$, there are a large smooth valley with comparatively bigger fluctuation and two sharp negative peaks at $N = 101$ and 146−147, respectively. The large smooth valley indicates that there is no structural transition with the growth of the clusters in this size range, and the two sharp peaks indicate that there are complete structures at these corresponding sizes. It can be seen from Figure 2 that the dominant motif is *m*-Dh, but the structural motif is fcc for Ag_{149}, Ag_{151}, Ag_{152}, and Ag_{158}. In Figure 4, positive peaks corresponding to the negative peak in Figure 3 can be clearly found, e.g., at Ag_{13}, Ag_{38}, Ag_{55}, Ag_{75}, and Ag_{101}. However, there are some other peaks at Ag_{19}, Ag_{64}, Ag_{71}, Ag_{108}, Ag_{117}, Ag_{126}, and Ag_{135} in the figure, which show that these clusters are stable ones compared with their neighboring clusters. With a detail examination, it can be found that the structures of Ag_{19}, Ag_{64}, Ag_{71}, Ag_{126}, and Ag_{135} are more symmetrical than their neighboring clusters, e.g., Ag_{19} with D_{5h} symmetry but Ag_{18} with C_2 symmetry and Ag_{20} with C_{2V} symmetry. Ag_{108} and Ag_{117} have the more stable structures than their neighboring clusters due to the structures changing from (3,2,2) *m*-Dh to (2,3,2) *m*-Dh.

However, the motif of Ih with a single central vacancy was indicated being stable at Ag_{146} and Ag_{147} in ref 37. To further investigate the results, the Ih core with a single central vacancy was used to optimize the structures of Ag_{146} and Ag_{147}. It was found that the same structure as above are obtained. On the other hand, in ref 11, the *m*-Dh motif has magic number at $N = 100$ with the corresponding (3,1,2) *m*-Dh structure. But there is no valley at $N = 100$ in Figure 3, and the putative stable structure is found to be (2,3,2) *m*-Dh with the potential energy −106.3212 for Ag_{100} in this work. For comparison, the energy of (3,1,2) *m*-Dh structure was calculated with Gupta potential and the result is −98.9675. Therefore, (2,3,2) *m*-Dh should be more reliable structure for Ag_{100}.

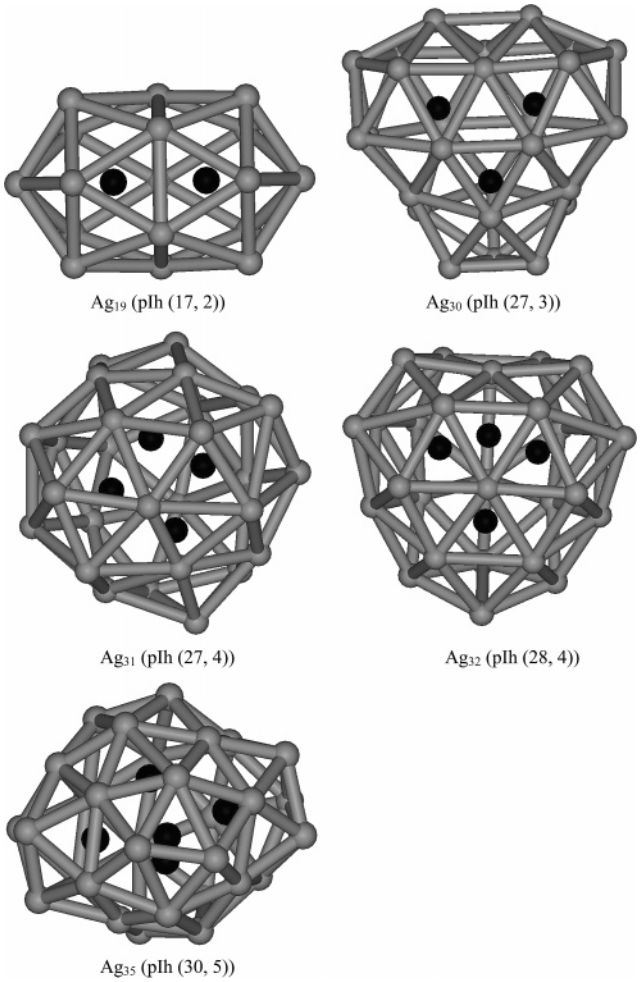

Figure 6. The structures of polyicosahedra motif. The atoms in the inner shell are shown in black.

3.3. Distribution of the Putative Stable Structures. The distribution of the Ag_{13-160} cluster structures is summarized in Table 1, including 28 amorphous structures, 13 Ih structures, 15 fcc structures, and 92 *m*-Dh structures in different sub-motifs.

Amorphous structures are obtained at the sizes of $N = 14-32$, 34−37, and 44−48. From Figure 2, it can be seen that these clusters have no symmetric axes. Among them, the structure of Ag_{15} is a complete icositetrahedron. It is classified into the amorphous motif for its scarceness. Furthermore, from Figure 2, it can also be found that the polyicosahedra (pIh)[38] motif can be obtained at Ag_{19}, Ag_{30-32}, and Ag_{35}. The structure of Ag_{19} has 30 facets, which is connected by two Ih structures with two atoms in the inner shell and 17 atoms in the outer shell, i.e., pIh (17, 2) as denoted in ref 38, and Ag_{20} has one more atom in outer shell than Ag_{19}. The structure of Ag_{30} is connected by three Ih, i.e., pIh (27, 3), the structures of Ag_{31} and Ag_{32} are connected by four Ih, i.e., pIh (27, 4) and pIh (28, 4), and the structure of Ag_{35} is connected by five Ih structures, i.e., pIh (30, 5). In order to more clearly demonstrate the structures of polyicosahedra motif, the structures of Ag_{19}, Ag_{20},

Ag_{28}, Ag_{30-32}, and Ag_{35} were shown in Figure 6. In Figure 6, bonds among the atoms in inner shell and between the inner shell and outer shell were not drawn.

Ih motif clusters are obtained at sizes of $N = 13$, 42, 49, 51−56, 58, 60, 61, and 147. Obviously, most of the clusters with Ih motif are around the magic number 55. The structure of Ag_{42} is a partial 55-atom Ih. The structures of Ag_{51}, Ag_{52}, and Ag_{53} are constructed by removing one, two, and three atoms from the out shell of Ag_{55}, and on the contrary, that of Ag_{56}, Ag_{58}, Ag_{60}, and Ag_{61} by adding one, three, five, and six atoms to the out shell, respectively. In Figure 2, Ag_{54} and Ag_{55} have the same top view, because Ag_{54} is constructed by only removing the center atom from Ag_{55}.

Including the TO motif, 15 structures with the fcc motif are obtained at 38−40, 50, 79, 80, 83, 85, 87 88, 90, 149, 151, 152, and 158. The structures of Ag_{38} and Ag_{79} are complete TO. Ag_{39}, Ag_{40}, Ag_{80}, and Ag_{85} have the same structural motif because these structure are constructed with one and two extra atoms to the out shell of Ag_{38}, and one and six extra atoms to the out shell of Ag_{79}, respectively. Furthermore, it can be seen that the atomic arrangement in the outer shell of Ag_{85} is different to the truncated octahedral motif.

From Table 1, it is obvious that the dominant motif of the clusters are *m*-Dh, especially when the size *N* is bigger than 57, and these *m*-Dh motif can be further divided into four sub-motifs of (2,2,2), (2,3,2), (3,2,2), and (3,3,2) *m*-Dh. The complete structures with these sub-motifs are found to be Ag_{75}, Ag_{101}, Ag_{146}, and Ag_{192}, respectively. In the small size range, only three clusters with (2,1,2) *m*-Dh motif at Ag_{33}, Ag_{41}, and Ag_{43}. The structures of Ag_{33}, Ag_{41}, and Ag_{43} are partial (2,1,2) *m*-Dh. Furthermore, from Table 1 and Figure 2, it can be seen that the structures with fcc and (2,2,2) *m*-Dh motif are alternately obtained in the range of Ag_{78} to Ag_{91}. Because 79 is a magic number of TO motif, fcc is the preferable motif for clusters around Ag_{79}. Then the preferable motif changes to (3,2,2) *m*-Dh at Ag_{92}, and back to (2,2,2) *m*-Dh at Ag_{93}. After Ag_{95}, the stable motif changes to (2, 3, 2) *m*-Dh in the range of $Ag_{96}-Ag_{119}$. So, from Ag_{96} to Ag_{119}, the stable structure is a result of the competition between (2,3,2) *m*-Dh and (3,2,2) *m*-Dh. After Ag_{119}, the dominant motif changes to (3,2,2) *m*-Dh. With the increase of the cluster size, four (3,3,2) *m*-Dh structures are obtained at the sizes of $N = 150$, 155, 157, and 159. Therefore, stable structures with *m*-Dh motif are a result of the competition among the sub-*m*-Dh motifs. Because the magic number of (3,3,2) *m*-Dh is 192, it should be predictable that this motif will be a dominant motif for the clusters of $N \geq 150$.

4. Conclusion

The structures of silver clusters from Ag_{121} to Ag_{160} were optimized with DLSc, which is a variation of the previous DLS method. The new optimized results of $Ag_{121-160}$ and our previous results of Ag_{13-120} were merged together to investigate the growth rule of silver clusters. A set of amorphous structures are obtained in the range of 13−48, together with several ordered structures at $N = 13$, 15, 33, 38−40, 41, and 43. In the size range of 49−61, the putative stable motif is Ih. The transition from Ih to Dh occurred in the size range of 57−62. Then, the putative stable motif change to *m*-Dh. On the hand, the stable structures of silver clusters with *m*-Dh motifs are found to be a result of the competition among the sub-*m*-Dh motifs.

Acknowledgment. This study is supported by National Natural Science Foundation of China (NNSFC) (Nos. 20325517 and 20573102) and the Ph.D. Programs Foundation of Ministry of Education (MOE) of China (No. 20050055001).

References and Notes

(1) Eachus, R. S.; Marchetti, A. P.; Muenter, A. A. The photophysics of silver halide imaging materials. *Annu. Rev. Phys. Chem.* **1999**, *50*, 117−144.

(2) Koretsky, G. M.; Knickelbein, M. B. The reactions of silver clusters with ethylene and ethylene oxide: infrared and photoionization strudies of $Ag_n(C_2H_4)_m$, $Ag_n(C_2H_4O)_m$ and their deuterated analogs. *J. Chem. Phys.* **1997**, *107* (24), 10555−10566.

(3) Kim, S. H.; Medeiros-Ribeiro, G.; Ohlberg, D. A. A.; Stanley-Williams, R.; Heath, J. R. Individual and collective electronic properties of Ag nanocrystals. *J. Phys. Chem. B* **1999**, *103*, 10341−10347.

(4) Wu, J.; Jiang, Y. S. Optimization of basis sets in valence bond calculations. *Chem. Phys. Lett.* **1999**, *311*, 315−320.

(5) Lee, I.; Han, S. W.; Kim, K. Production of Au-Ag Alloy nanoparticles by laser ablation of bulk alloys. *Chem. Commun.* **2001**, 1782−1783.

(6) Johnston, R. L. Evolving better nanoparticles: genetic algorithms for optimising cluster geometries. *J. Chem. Soc. Dalton Trans.* **2003**, *22*, 4193−4207.

(7) Marks, L. D. Experimental studies of small particle structures. *Rep. Prog. Phys.* **1994**, *57*, 603−649.

(8) Martin, T. P. Shells of atoms. *Phys. Rep*. **1996**, *273*, 199−241.

(9) Hall, B. D.; Flüeli, M.; Monot, R.; Borel, J. P. Multiply twinned structures in unsupported ultrafine silver particles observed by electron diffraction. *Phys. Rev. B* **1991**, *43* (5), 3906−3917.

(10) Reinhard, D.; Hall, B. D.; Ugarte, D.; Monot, R. Size-independent fcc-to-icosahedral structural transition in unsupported silver clusters: An electron diffraction study of clusters produced by inert-gas aggregation. *Phys. Rev. B* **1997**, *55* (12), 7868−7881.

(11) Baletto, F.; Mottet, C.; Ferrando, R. Reentrant morphology transition in the growth of free silver nanoclusters. *Phys. Rev. Lett.* **2000**, *84* (24), 5544−5547.

(12) Baletto, F.; Ferrando, R. Structural properties of nanoclusters: energetic, thermodynamic, and kinetic effects. *Rev. Mod. Phys*. **2005**, *77* (1), 371−423.

(13) Heer, W. A. The physics of simple metal clusters: experimental aspects and simple models. *Rev. Mod. Phys.* **1993**, *65* (3), 611−676.

(14) Baletto, F.; Mottet, C.; Ferrando, R. Microscopic mechanisms of the growth of metastable silver icosahedra. *Phys. Rev. B* **2001**, *63*, 155408−1−10.

(15) Baletto, F.; Ferrando, R.; Fortunelli, A.; Montalenti, F.; Mottet, C. Crossover among structural motifs in transition and noble-metal clusters. *J. Chem. Phys.* **2002**, *116* (9), 3856−3863.

(16) Tian, Z.-M.; Tian, Y.; Wei, W.-M.; He, T.-J.; Chen, D.-M.; Liu, F.-C. Ab initio study on the kinetics and mechanisms of the formation of Ag_n (n=2−6) clusters. *Chem. Phys. Lett.* **2006**, *420*, 550−555.

(17) Matulis, V. E.; Ivashkevich, O. A.; Gurin, V. S. DFT study of electronic structure and geometry of neutral and anionic silver clusters. *J. Mol. Struct.* **2003**, *664*, 291−308.

(18) Patrick, W.; Thomas, B.; Stefan, G.; Manfred, M. K. Structures of small silver cluster cations (Ag_n^+, n<12): ion mobility measurements versus density functional and MP_2 calculation. *Chem. Phys. Lett.* **2002**, *355*, 355−364.

(19) René, F. Theoretical study of the structure of silver clusters. *J. Chem. Phys*. **2001**, *115* (5), 2165−2177.

(20) Erkoç, Ş.; Yılmaz, T. Molecular-dynamics simulations of silver clusters. *Phys. E* **1999**, *5*, 1−6.

(21) Doye, J. P. K.; Wales, D. J. Global minima for transition metal clusters described by Sutton-Chen potentials. *New. J. Chem.* **1998**, *22*, 733−744.

(22) Michaelian, K.; Rendón, N.; Garzón, I. L. Structure and energetics of Ni, Ag and Au nanoclusters. *Phys. Rev. B* **1999**, *60* (3), 2000−2010.

(23) Shao, X. G.; Liu, X. M.; Cai, W. S. Structural optimization of silver clusters up to 80 atoms with Gupta and Sutton-Chen potentials. *J. Chem. Theor. Comput.* **2005**, *1*, 762−768.

(24) Zhan, H.; Cheng, L. J.; Cai, W. S.; Shao, X. G. Structural optimization of silver clusters form Ag_{61} to Ag_{120} by dynamic lattice searching method. *Chem. Phys. Lett.* **2006**, *422*, 358−362.

(25) Shao, X. G.; Cheng, L. J.; Cai, W. S. A dynamic lattice searching method for fast optimization of Lennard-Jones clusters. *J. Comput. Chem.* **2004**, *25*, 1693−1698.

(26) Cheng, L. J.; Cai, W. S.; Shao, X. G. Geometry optimization and conformational analysis of $(C60)_N$ clusters by using a dynamic lattice searching method. *Chem. Phys. Chem.* **2005**, *6*, 261−266.

(27) Yang, X. L.; Cai, W. S.; Shao, X. G. A dynamic lattice searching method with constructed core for optimization of large Lennard-Jones clusters. *J. Comput. Chem* **2007**, *28* (8), 1427−1433.

(28) Cleveland, C. L.; Landman, U.; Schaaff, T. G.; Shafigullin, M. N.; Stephens, P. W.; Whetten, R. L. Structural evolution of smaller gold nanocrystals: the truncated decahedral motif. *Phys. Rev. Lett.* **1997**, *79* (10), 1873−1876.

(29) Jiang, H. Y.; Cai, W. S.; Shao, X. G. New lowest energy sequence of Mark's decahedral Lennard-Jones clusters containing up to 10000 atoms. *J. Phys. Chem. A* **2003**, *107* (21), 4238−4243.

(30) Xiang, Y. H.; Jiang, H. Y.; Cai, W. S. An efficient method based on lattice construction and the genetic algorithm for optimization of large Lennard-Jones clusters. *J. Phys. Chem. A* **2004**, *108*, 3586−3592.

(31) Jacobsen, K. W.; Norskov, J. K.; Puska, M. J. Interatomic interactions in the effective-medium theory. *Phys. Rev. B* **1987**, *35*, 7423−7442.

(32) Ercolessi, F.; Parrinello, M.; Tosatti, E. Simulation of gold in the glue model. *Philos. Mag. A* **1988**, *58*, 213−218.

(33) Daw, M. S.; Baskes, M. I. Embedded-atom method: derivation and application to impurities, surfaces, and other defects in metals. *Phys. Rev. B* **1984**, *29*, 6443−6453.

(34) Sutton, A. P.; Chen, J. Long-range Finnis-Sinclair potentials. *J. Philos. Mag. Lett.* **1990**, *61*, 139−146.

(35) Rosato, A.; Guillope, M.; Legrand, B. Thermodynamical and structural- properties of FCC transition-metals using a simple tight-binding model. *Philos. Mag. A* **1989**, *59*, 321.

(36) Gupta, R. P. Lattice relaxation at a metal surface. *Phys. Rev. B* **1981**, *23*, 6266−6270.

(37) Mottet, C.; Tréglia, G.; Legrand, B. New magic numbers in metallic clusters: an unexpected metal dependence. *Surf. Sci.* **1997**, *383*, L719−L727.

(38) Rossi, G.; Rapallo, A.; Mottet, C.; etc. Magic polyicosahedral core-shell clusters. *Phys. Rev. Lett.* **2004**, *93* (10), 105503.